A BIOMECHANICAL MODEL OF THE BREAST TO TRACK TUMOURS

J.H. Chung*, V. Rajagopal*, P.M.F. Nielsen* and M.P. Nash*

* Bioengineering Institute, The University of Auckland, Auckland, New Zealand

jh.chung@auckland.ac.nz

Abstract: A number of biomechanical models of the breast have been developed to enable accurate location of suspicious features using multiple imaging technologies. Mammograms provide 2D representations of highly deformed 3D breasts. Accurate co-location of suspicious features from multiple mammograms is a non-trivial task. In this work, we present a novel method based upon the physics of large deformation mechanics to interpret mammogram containing suspicous features in order to accurately co-locate them in 3D space.

Introduction

There exist a number of screening and diagnostic tools available for breast cancer. Mammography is currently the gold standard for its highly sensitive nature in detecting carcinomas containing microcalcifications [1]. However, mammograms are 2D representations of a 3D object, and each mammogram is taken with a different deformed breast state (typically mediolateral-oblique and cranio-caudal views are used). These limitations pose difficulties for clinicians attempting to accurately locate suspicious masses in the undeformed breast state.

In this study, we present a novel method to interpret mammograms using a biomechanical model based on the laws of physics in order to predict the location of an abnormal mass from mammograms in 3D space. Phantom studies using a homogeneous and isotropic deformable material are validated against experimental results.

Biomechanical Model of the Breast

During mammographic procedures, a patient's breast undergoes strains of up to 50%. In order to model such large deformations of the breast, finite elasticity theory must be used to accurately describe the kinematics of tissue movement. In this section, a brief summary of the theory is depicted. Readers are referred to [2] and [3] for details.

Kinematics

Let us assume that a deformable body undergoes a general motion, from a reference (or stress-free) state with coordinates $\boldsymbol{X}$ to a deformed state with coordinates $\boldsymbol{x}$. The deformation gradient tensor $\boldsymbol{F}$ maps a line segment in the reference configuration into a line segment in the deformed configuration, where

$$\boldsymbol{F} = \frac{\partial \boldsymbol{x}}{\partial \boldsymbol{X}} \tag{1}$$

Using this deformation gradient tensor, we can define the *Green-Lagrange strain tensor,* $\boldsymbol{E}$, where

$$\boldsymbol{E} = \frac{1}{2}\left(\boldsymbol{F}^T\boldsymbol{F} - \boldsymbol{I}\right) \tag{2}$$

where $\boldsymbol{I}$ is the identity matrix. Calculation of stress tensors may be achieved by differentiating a strain energy function W with respect to $\boldsymbol{E}$.

Constitutive Laws

Sylgard® silicon gel (Dow Corning, USA) was used to create a phantom model of the breast to validate our computational compression studies. Previous research [4], [5] has shown that the neo-Hookean constitutive law accurately represents the mechanical behaviour of this incompressible, isotropic gel. For such a material, the strain energy function W is defined as

$$W = c_1\,(I_1 - 3) \tag{3}$$

where c_1 is determined experimentally and I_1 is the 1^{st} invariant (trace) of $\boldsymbol{F}^T\boldsymbol{F}$.

The 2^{nd} Piola-Kirchhoff stress tensor $\boldsymbol{S}$ is evaluated by differentiating the strain energy function with respect to the *Green-Lagrange strain tensor,* $\boldsymbol{E}$.

$$\boldsymbol{S} = \frac{\partial W}{\partial \boldsymbol{E}} \tag{4}$$

We enforced first derivative continuity of both geometry and deformation by using cubic-Hermite interpolation functions. This approach ensured that the stress and strain fields remained continuous, improving the rate of solution convergence [6].

Governing Equation: Principle of Virtual Work

The equations of motion can be obtained by balancing forces acting on the body

$$\mathrm{div}\sigma + \mathbf{b} = \rho\ddot{\mathbf{u}} \tag{5}$$

where σ is the Cauchy stress, $\mathbf{b}$ is the body force, ρ is the density and $\ddot{\mathbf{u}}$ is the acceleration. The Cauchy stress

ISSN: 1727-1983

can be evaluated using the 2^{nd} Piola-Kirchhoff stress tensor found in equation (4)

$$\sigma = \frac{1}{J}\boldsymbol{F}\boldsymbol{S}\boldsymbol{F}^{T} \tag{6}$$

where J=det($\boldsymbol{F}$)

The principle of virtual work is used to convert this strong form of the governing equations into a weak form, expressed in terms of integrals rather than differential equations. In this form, numerical methods such as the finite element method can be used to solve equations.

$$\int_s \mathbf{t}\cdot\delta\mathbf{u}ds + \int_v \mathbf{b}\cdot\delta\mathbf{u}dv = \int_v \sigma : \frac{\partial(\delta\mathbf{u})}{\partial \boldsymbol{x}}dv + \int_v \rho\ddot{\mathbf{u}}\cdot\delta\mathbf{u}dv \tag{7}$$

where $\delta\mathbf{u}$ is the virtual displacement and $\mathbf{t}$ is the surface traction. Note that the integrations are performed on the current configuration (surface ds or volume dv). For a quasi-static problem, the term on the right-hand side involving the acceleration is neglected, and we obtain a nonlinear residual equation,

$$\mathbf{R} = \int_v \sigma : \frac{\partial(\delta\mathbf{u})}{\partial \boldsymbol{x}}dv - \int_s \mathbf{t}\cdot\delta\mathbf{u}ds - \int_v \mathbf{b}\cdot\delta\mathbf{u}dv = \mathbf{0} \tag{8}$$

This system of residual equations may be solved using nonlinear iterative algorithms such as the Newton-Raphson method. The tangent stiffness matrix, $\mathbf{K}$ may be approximated using finite difference estimates of the residual derivatives

$$K_{mn} \approx \frac{R_m(\boldsymbol{x}_i + \Delta\boldsymbol{e}_n) - R_m(\boldsymbol{x}_i)}{\Delta\boldsymbol{e}_n} \tag{9}$$

The deformed geometry, $\boldsymbol{x}$, is initially set to $\boldsymbol{X}$ and the next set of solutions are calculated by adding the deformation increment $\boldsymbol{u}$ to the current $\boldsymbol{x}_i$. The deformation increment is calculated by solving

$$\mathbf{K}\boldsymbol{u} = -\mathbf{R}(\boldsymbol{x}_i); \qquad \boldsymbol{x}_{i+1} = \boldsymbol{x}_i + \boldsymbol{u} \tag{10}$$

This process is repeated until equation (8) satisfies a set of error conditions.

Contact Mechanics

It is difficult to track material points of the breast tissue during mammographic compression. Hence we cannot apply simple displacement boundary conditions. To cope with unknown boundary displacements, we used contact mechanics based upon a frictional cross-constraint method. The residual equation in equation (8) is modified with contact constributions by

$$\mathbf{R}_{\text{global}} = \mathbf{R} - \int_{S^c} f_{\text{N}}(\delta\mathbf{u}_{\text{slave}} - \delta\mathbf{u}_{\text{master}})\cdot\mathbf{n}dS^c - \sum_{\alpha=1}^{2}\int_{S^c} f_{\text{T}_\alpha}(\delta\mathbf{u}_{\text{slave}} - \delta\mathbf{u}_{\text{master}})\cdot\mathbf{t}_\alpha dS^c \tag{11}$$

where S^c is the slave or contact surfaces (deformable breast), $\mathbf{n}$ is the normal vector at the master surface (rigid plates) and $\mathbf{t}_\alpha$ are two tangential vectors at the master surface. The normal force f_{N} and the tangential forces f_{T_α} are evaluated as defined in [7].

Phantom Studies: Validation of Cranio-caudal and Mediolateral Compressions

We conducted a series of experimental studies on a silicon gel phantom in order to validate our model predictions against the experimental surface-scanned data. We used a simplified symmetric geometry (see Figure 1, width = 80 mm, depth = 120 mm, height=160 mm). The material properties of the silicon gel had been estimated in [8], where a neo-Hookean material law was used with $c_1 = 0.426\ kPa$. Each mammographic compression was simulated using this material law, and compared against the experimental surface geometry recorded using the FASTSCAN$^{\text{TM}}$ (Polhemus, UK).

Cranio-caudal (CC) compression

CC compression was performed with the phantom placed in a supine orientation. Two rigid plates were used to compress the phantom to 50 mm thickness (37.5% compression). Figure 1 depicts the simulation result and its comparsion with the surface data of the compressed phantom.

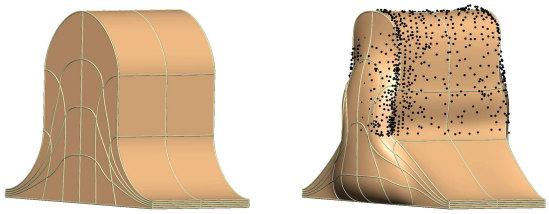

Figure 1: The phantom in supine position subject to CC compression. Left: the undeformed configuration. Right: the compressed model (surface) with the surface-data scanned from the experiment (dots).

The global root-mean-squared (RMS) value between the predicted deformed surface and the recorded data points was 1.61 mm for the CC compression.

Mediolateral (ML) compression

ML compression was performed with the phantom oriented on its side. ML compression was preferred to mediolateral-oblique (MLO) compression for this phantom study due to its geometric symmetry in the mediolateral direction. The phantom was compressed to 50 mm thickness (37.5% compression). Figure 2 depicts the simulation result and its comparsion with the surface data of the compressed phantom.

ISSN: 1727-1983

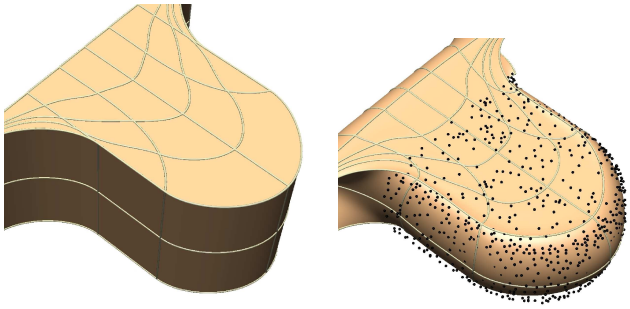

Figure 2: The phantom oriented on its side subject to ML compression. Left: the undeformed configuration. Right: the compressed model (surface) with the surface-data scanned from the experiment (dots).

The global RMS value between the predicted deformed surface and the recorded data points was 1.65 mm for the ML compression.

Interpretation of Mammograms Using The Biomechanical Model: A Demonstration

From the compression simulations, we generated artificial mammograms from each of the deformed models. Let us assume that an abnormality (5 mm by 5 mm) was identified in both mammograms, as illustrated in Figure 3.

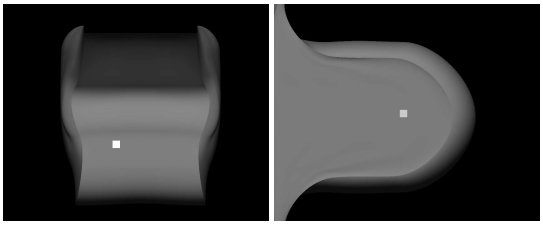

Figure 3: Simulated CC (left) and ML (right) mammograms generated from the simulation results. An abnormalities (white square) is included.

We can thus identify a set of material points which are possible candidates for this tumour on each deformed breast model. Locations of these points are tracked to the undeformed breast state, according to the underlying laws of physics used to simulate the deformations (Figure 4).

This will give two sets of material points within the undeformed phantom that are candidates for the abnormalty. Then the tumour may be localised by simply taking the intersection of the two candidate sets (Figure 5).

With this information, we can simulate any other deformation required for other image modalities, such as MRI, CT, and ultrasound, and track the located tumour in the deformed breast geometry through a simple forward solution. For example, a patient's breast may be in a

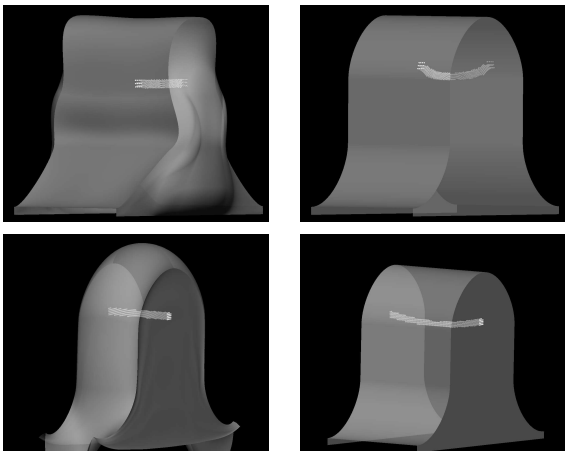

Figure 4: Top: set of material points corresponding to the region of interest shown in the simulated CC mammogram (left) and their locations in the undeformed breast (right). Bottom: similar procedure as above, but for ML mammogram.

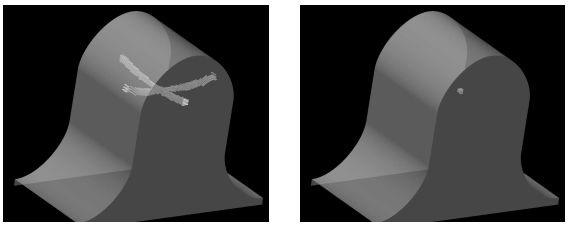

Figure 5: Left: The set of abnormality candidates identified from the mammograms, in the undeformed phantom geometry. Right: The intersection of these sets is the unique mass.

prone position during a magnetic resonance (MR) imaging procedure and such a deformation can be predicted using this model to accurately determine the 3D location of the tumour (Figure 6).

Discussion

In this study, a modelling framework has been proposed to interpret mammograms using an accurate biomechanical model. We have demonstrated the accuracy of the model to simulate mammographic compressions (CC and ML) by comparison with experiments on phantoms. Using the model predictions for both compressions, CC and ML mammograms were artificially generated with a manifest abnormality. The material points in each deformed state, due to the abnormalty, were tracked to the locations in the undeformed breast geometry. The abnormalty was localised by taking the intersection of the tracked material points.

It is important to note that the set of material points in the deformed breast becomes warped in the undeformed breast. Clinically, lesions are localised by using a per-

ISSN: 1727-1983

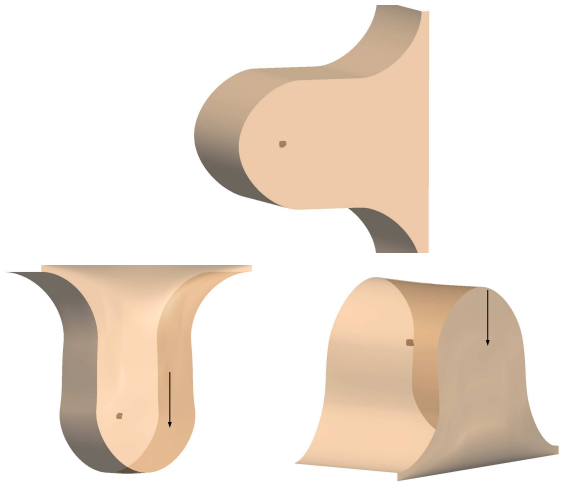

Figure 6: Tracking the tumour (dots) in the breast under prone-gravity loading conditions (left) and also under supine-gravity loading conditions (right) from the undeformed unloaded breast state (top). Arrows indicate the direction of gravity acting on the model.

forated or marked compression plate [1]. The point of needle insertion on the skin is chosen according to the coordinates of the tumour in each of the mammograms with reference to anatomical markings (usually the nipple). The needle is then inserted beyond the depth measured from the CC mammogram. The warping of the material points in the undeformed breast indicates that the current clinical approach of localising tumours might not be appropriate and needs to account for this warping effect due to the compressive deformation.

We are in the process of validating this registration method, by inserting a foreign material into the phantom to mimic the presence of a tumour. Evaluation of its location in the undeformed phantom will require the use of imaging techniques such as MR. These phantom studies will provide the foundations for this tumour tracking technique. Further validation studies are required in order to account for greater anantomical realism, such as the effects of skin, different breast tissue material properties, and patient-specific breast geometries. These anatomically realistic details will be built into the phantom studies, making them more relevant for clinical purposes.

References

[1] H.HEYWANG-KOBRUNNER SYLVIA, D.DAVID DERSHAW, and INGRID SCHREER. *Diagnostic Breast Imaging*. Thieme, 2 edition, 2001.

[2] J. BONET and R.D. WOOD. *Nonlinear Continuum Mechanics for Finite Element Analysis*. Cambridge University Press, 1997.

[3] P. WRIGGERS. *Computational Contact Mechanics*. Wiley, 2002.

[4] K.F. AUGENSTEIN, B.R. COWAN, I.J. LEGRICE, P.M.F. NIELSEN, and A.A. YOUNG. Method and apparatus for soft tissue material parameter estimation using tissue tagged magnetic resonance imaging. *Journal of Biomechanical Engineering*, 127:148–157, 2005.

[5] V. RAJAGOPAL, P.M.F. NIELSEN, and M.P. NASH. A 3D finite element model of the breast to study breast cancer. In *WC2003 World Congress on Medical Physics and Biomedical Engineering*, 8 2003.

[6] J. ODEN. *Finite Elements of Nonlinear Continua*. McGraw-Hill, Inc, 1972.

[7] G. ZAVARISE, P. WRIGGERS, and B.A. SCHREFLER. A method for solving contact problems. *International Journal for Numerical Methods in Engineering*, 42:473–498, 1998.

[8] J.H. CHUNG, V. RAJAGOPAL, P.M.F. NIELSEN, and M.P. NASH. Computational modeling of the breast during mammography for tumor tracking. In *Medical Imaging 2005: Physiology, Function and Structure from Medical Images*, volume 5746, pages 817–824. SPIE, 2005.

ISSN: 1727-1983